Available online at www.sciencedirect.com
ScienceDirect
Trans. Nonferrous Met. Soc. China 34(2024) 139−156
Transactions of Nonferrous Metals Society of China
www.tnmsc.cn

Discharge channel structure revealed by plasma electrolytic oxidation of AZ31Mg alloy with magnetron sputtering Al layer and corrosion behaviors of treated alloy

Pan-feng HU, Bing-jian WEI, Yu-lin CHENG, Ying-liang CHENG

College of Materials Science and Engineering, Hunan University, Changsha 410082, China

Received 6 July 2022; accepted 6 October 2022

Abstract: Plasma electrolytic oxidation (PEO) of AZ31 magnesium alloy with a thin magnetron sputtering Al layer was carried out in a silicate–hexametaphosphate electrolyte to investigate the PEO mechanism and improve the corrosion resistance of the alloy. SEM and EDS were employed to examine the coating morphology and trace the Mg and Al elements in the coatings. It is found that new coating is mainly formed at the lower part of the discharge channels close to the interface of coating/metal substrate. The previously formed oxides at the upper part of discharge channels are largely kept in their original solid forms within the discharge channels. Only a small fraction of the molten oxide flows out through the micropores of the coating, reaching the top layer. The anionic species can freely access the innermost of the coatings, which are also transported through the electrolyte-filled pores. The corrosion behavior of the coatings was examined by open circuit potentials, polarization curves and EIS tests in 3.5 wt.% NaCl. Owing to its compact nature, the magnetron sputtered Al layer can significantly improve the corrosion resistance of the AZ31 Mg alloy, which is even better than that of the samples after PEO treatment.

Key words: AZ31 magnesium alloy; magnetron sputtering Al layer; plasma electrolytic oxidation; discharge channel; corrosion resistance

1 Introduction

Magnesium alloys are the lightest structural metal materials, which are attractive in applications where weight reduction is a priority, such as aerospace and automotive industries [1−3]. However, the poor corrosion and wear resistances of magnesium alloys limit their wide application [4−6].

Surface treatment technologies, such as magnetron sputtering [7], arc spraying [8], hot dip aluminized plating [9] and plasma electrolytic oxidation (PEO) [10], have been widely used to improve the surface properties of a variety of metals and alloys. However, the melting points of magnesium alloys are too low, so arc spraying and hot-dip aluminizing are not suitable for them. The magnetron sputtering technology can be carried out at relatively lower temperatures (250−400 °C) or even room temperature [11]. WEI et al [12] prepared a magnetron sputtering Al layer on AZ31 magnesium alloy, and then through subsequent PEO treatment, the wear resistance of AZ31 magnesium alloy was effectively improved. However, the quality of the magnetron sputtered layer was not high enough, and the plated Al layer lost its protection after soaking in NaCl for 5 h. Hence, deposition of high-quality layer or combination with other post treatment methods, e.g. PEO, is essential for the magnetron sputtering treatment of magnesium alloys.

PEO is a new surface treatment method to

Corresponding author: Ying-liang CHENG, Tel: +86-731-88821727, Fax: +86-731-88823554, E-mail: chengyingliang@hnu.edu.cn
DOI: 10.1016/S1003-6326(23)66387-3

improve the surface properties of various metals (Al, Mg, Ti, Zr, Ta, Cu, etc.) and their alloys by forming ceramic coatings under plasma discharges [13−20]. PEO has the advantages of using environmentally friendly alkaline electrolytes, requiring little or no pretreatment, and the capability to handle workpieces with complex shapes [21,22]. However, a lack of in-depth understanding of the PEO mechanisms restricts further development of the technology. Plasma discharges play a decisive role in PEO coating formation. The temperature of the plasma discharges can reach 3000−7000 K [23−25]. Under the melting−quenching effect, new oxides are formed within the discharge channels [26−28]. PEO coatings are often featured by the so-called pancake structures, with a hole usually being found in the center of each pancake structure [23,28]. SUNDARARAJAN and RAMA KRISHNA [29] believed that the hole was the discharge channel, "through which the molten alumina flowed out of the channel and rapidly solidified leaving the sharp and distinctly visible boundaries thus delineating each pancake". However, others believe that the whole pancake structure is a discharge channel, with the central hole formed by gas ventilation [23]. TU et al [28] had traced the distribution of tungsten element in the PEO coatings on magnesium alloy and proposed a discharge model with molten oxide distributed at the bottom of a discharge channel. GAO et al [30] also proposed a model of the microstructure of the discharge channel by Ti tracer, which consists of groove-like oxidation region at the coating/substrate interface, cylinder-shaped discharge channel in the compact coating, and trumpet-shaped channel in the outer porous coating.

The difficulty in discharge channel micro-structure study originates from the transient nature of the discharges. A typical discharge lifetime usually lasts from several microseconds to a few hundred microseconds and the individual discharges tend to occur in "cascades" at some particular locations [31,32]. Owing to the short discharge time, the details of the discharge channel are difficult to detect. For instance, although the electron temperature of the plasma discharges based on optical emission spectroscopy (OES) study is much higher than the melting point of most metals and ceramics, we are not sure whether the coating oxides will be completely re-melted after a plasma discharge. STOJADINOVIC et al [33] believed that the high melting point of tantalum (3017 °C) prevents the formation of metallic plasma in PEO of the metal. The formed oxides of MgO and Al_2O_3 in the PEO of common lightweight metals also have high melting points, so it is interesting to know the state of these oxides within the discharge channels.

In this study, a dense magnetron sputtered Al film was first prepared on the surface of AZ31 magnesium alloy, and then the Al-coated alloy was PEO-treated for different time in a silicate/hexametaphosphate electrolyte. The aim of this study is to improve the corrosion resistance of the magnesium alloy by forming a higher quality magnetron sputtering layer and to obtain the information about the discharge channels by tracing the distribution of the different substrate metal elements in the coatings.

2 Experimental

An ~5 mm-thick rolled plate of AZ31 Mg alloy (nominal composition in wt.%: Al 2.7−3.0, Zn 0.8−1.0, Mn 0.3−0.5, Si 0.1, Fe 0.05, Cu 0.05 and Mg balance) was used. The AZ31 Mg alloy was cut into specimens in dimensions of 20 mm × 10 mm × 5 mm. Then, they were sequentially ground down to 5000# SiC paper, and polished with 3.5 μm diamond paste. After polishing, the specimens were degreased with ethanol, rinsed with distilled water and dried and stored in a desiccator ready for magnetron sputtering. An Al layer of ~11 μm was deposited on the surface of the specimens by DC magnetron sputtering at a commercial company. In the magnetron sputtering process, 99.9% pure aluminum target was utilized, the power supply had a capacity of 200 W, the deposition rate was 5 Å/s, and the deposition time was 7 h. Other information is unknown due to confidentiality. In our previous studies, magnetron sputtering layers of Al were also fabricated on AZ31 magnesium alloy [12] and Ti6Al4V [34], but with different process parameters. After magnetron sputtering, each specimen was connected to a copper wire and sealed with epoxy resin, leaving the magnetron sputtered surface exposed for subsequent PEO treatment.

The PEO power supply and the experimental arrangement were the same as those in Ref. [35]. PEO treatment was carried out in a 1 L glass vessel, equipped with magnetic stirring and a water-cooling system. The electrolyte was 12 g/L Na_2SiO_3 + 15 g/L

$(NaPO_3)_6$ + 1 g/L KOH, prepared from high purity chemicals and distilled water. Pulsed bipolar constant current regime with 1000 Hz frequency and 20% duty cycle was employed. An oscilloscope (Tektronix TDS 1002C−SC) was used to monitor the current waveforms. The average positive and negative current densities used for PEO were ~0.16 and ~0.08 A/cm^2, respectively. The coatings were formed for 5, 10, and 60 min, respectively.

Scanning electron microscope (SEM, ZEISS EVO) combined with energy dispersive spectrometer (EDS, OXFORD) and X-ray diffractometer (XRD, Rigaku D/MAX 2500, Cu K_α radiation, Bragg−Brentano geometry) were used to examine the morphology, composition and phase composition of the PEO coatings, respectively.

The corrosion behavior of samples was evaluated by electrochemical methods in 3.5 wt.% NaCl solution. Open circuit potential (OCP), potentiodynamic polarization and electrochemical impedance spectroscopy (EIS) were operated under a three-electrode configuration. Samples to be tested are the working electrodes. A piece of platinum plate and a saturated calomel electrode (SCE) were used as the counter electrode and reference electrode, respectively. OCPs were first recorded for 1 h, and then potentiodynamic polarization tests were performed, using a scan rate of 0.5 mV/s from −0.5 to 1.5 V with respect to the OCP. The EIS spectra were recorded after immersion for 1, 3 and 5 h, respectively. The EIS tests were performed using sinusoidal signals with amplitude of 10 mV around the OCP and the scanning frequency range was from 1×10^5 Hz to 0.005 Hz. The EIS data were fitted by ZSimpWin software.

3 Results

3.1 Magnetron-sputtered Al layer

The surface and cross-sectional morphologies of the magnetron sputtering Al layer are presented in Fig. 1. Figure 1(a) shows that aluminum grains with different sizes are uniformly deposited on the surface and each Al grain shows a “pyramid-like” shape. The size of a medium grain is about 1.65 μm. The grains are closely arranged, and there are no obvious cracks on the surface of the aluminized layer, but only a few tiny gaps. The grain size of the magnetron sputtering Al layer in this study is significantly smaller than that in our earlier work [12], which has large grains up to 4.8 μm. Figure 1(b) shows the cross-section of the Al layer, which is ~11 μm in thickness. There are no obvious defects such as pores in the cross section, and the interface between the Al/AZ31 magnesium alloy substrate is smooth and has no obvious gaps.

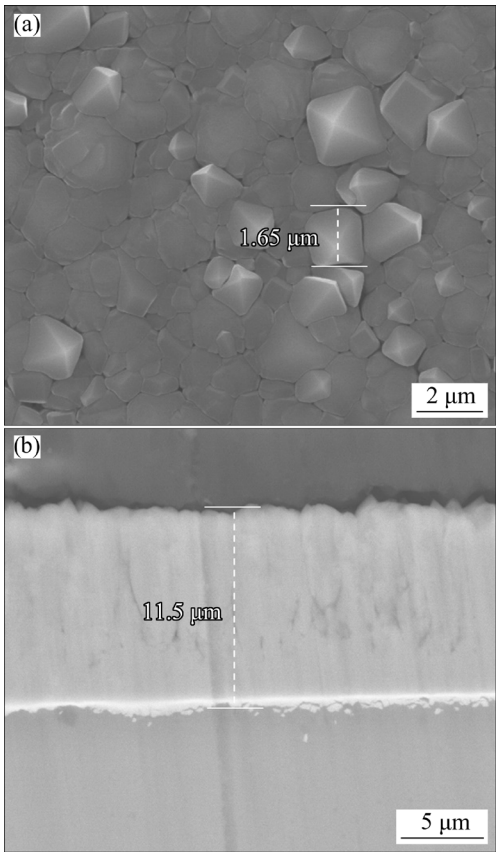

Fig. 1 Scanning electron micrographs showing morphology of magnetron sputtered Al layer on AZ31 magnesium alloy: (a) Surface; (b) Cross-section

3.2 Cell potential−time responses

The variation of the cell potential during the PEO treatment of the Al-coated AZ31 magnesium alloy in the 12 g/L Na_2SiO_3 +15 g/L $(NaPO_3)_6$ + 1 g/L KOH electrolyte is shown in Fig. 2. The negative potential is recorded in absolute values. In the first 18 s, the positive potential rapidly rises to 400 V, which corresponds to the formation of an anodic film. After that, the potential reaches the breakdown potential, with sparks being observed on the surface of the sample, and the rate of potential rising decreases. There is a small increase in the anodic potential during 11−14 min, and then the potential increases slowly to the final voltage of 584 V at 60 min. The negative potential is similar to

that of positive potential, but with lower values. The negative potential shows an obvious inflexion at ~11 min, after which the potential rises gradually to a final value of −206 V.

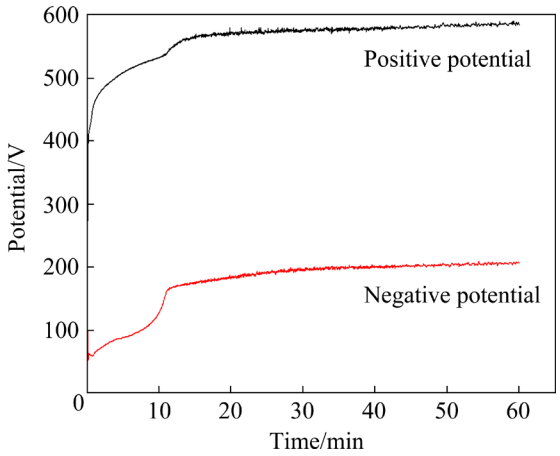

Fig. 2 Cell potential−time responses during PEO of Al−AZ31 duplex system (Absolute values are given for the negative potential)

3.3 SEM morphologies

Figure 3 shows the surface and cross-sectional morphologies of the duplex Al−AZ31 magnesium alloy after 5 min PEO treatment. In Fig. 3(a), there are many pancake-like structures on the surface. The size of the pancake structures varies, and the larger one is about 15 μm. Micro-cracks, as a result from the releasing of thermal stress during the cooling of the discharge channels, exist on the surface of the PEO coating. EDS analysis of Point A on a pancake structure in Fig. 3(a) shows a composition (at.%) of O 51.1, Al 48.4, and Si 0.6. Therefore, the pancake structure is mainly composed of alumina. Careful observation shows that there are fine particles around the pancake structures. These fine particles are formed by the deposition of electrolyte components. EDS shows that they mainly contain Si and P elements.

Figure 3(b) shows cross-sectional morphology of the sample. It can be seen that the PEO layer co-exists with the magnetron sputtering Al layer. The total thickness of the PEO coating and Al layer is about 13.4 μm, indicating that the thickness increases after the Al layer is converted into PEO coating. The thickness of the unconsumed Al layer is 6.5−8 μm. There are pores with different sizes in the cross section of PEO coating. Overall, the PEO coating, the magnetron sputtered Al layer and the AZ31 substrate are well bonded with each other. EDS shows that the PEO coating are composed of Al, O and a small amount of Si and P. At this stage, the magnesium alloy substrate has not yet participated in the formation of PEO coating.

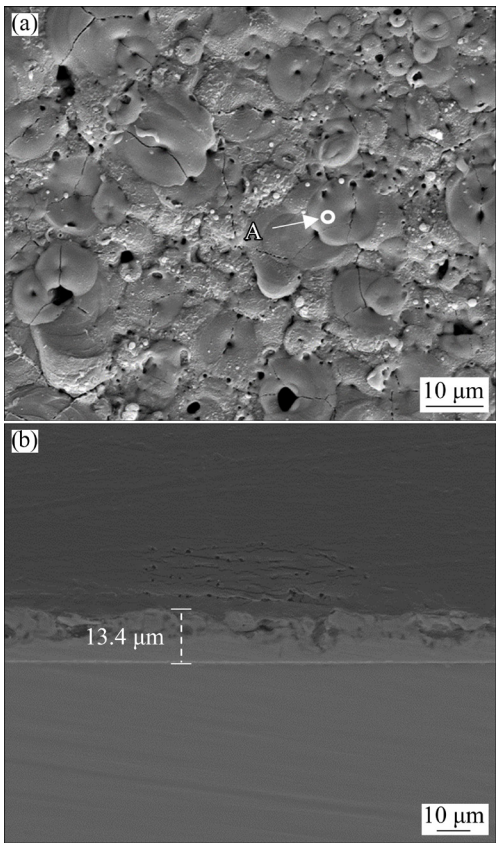

Fig. 3 Scanning electron micrographs showing surface (a) and cross-section (b) of coating formed after 5 min PEO treatment on Al−AZ31 magnesium alloy

Figure 4 shows the surface morphology and elemental mapping of the sample after 10 min PEO treatment. The surface of the coating is still featured by pancake structures, and the size of the pancakes has grown to ~22 μm. Compared with the 5 min coating, the number of pores is significantly reduced. The EDS analysis at Point A of the pancake structure in the secondary electron image shows the composition (at.%) of O 40.9, Al 32.8, Mg 17.4, and Si 8.8. The result shows that at this location, the Mg element from the substrate has reached the surface of the coating. The elemental mapping shows that at this time, most of the surface area is still the original Al oxide, and Mg only appears in some particular positions. The mapping of Si shows that Si element tends to be enriched around the pancake structure. The point analysis shows no P element on the coating surface, possibly

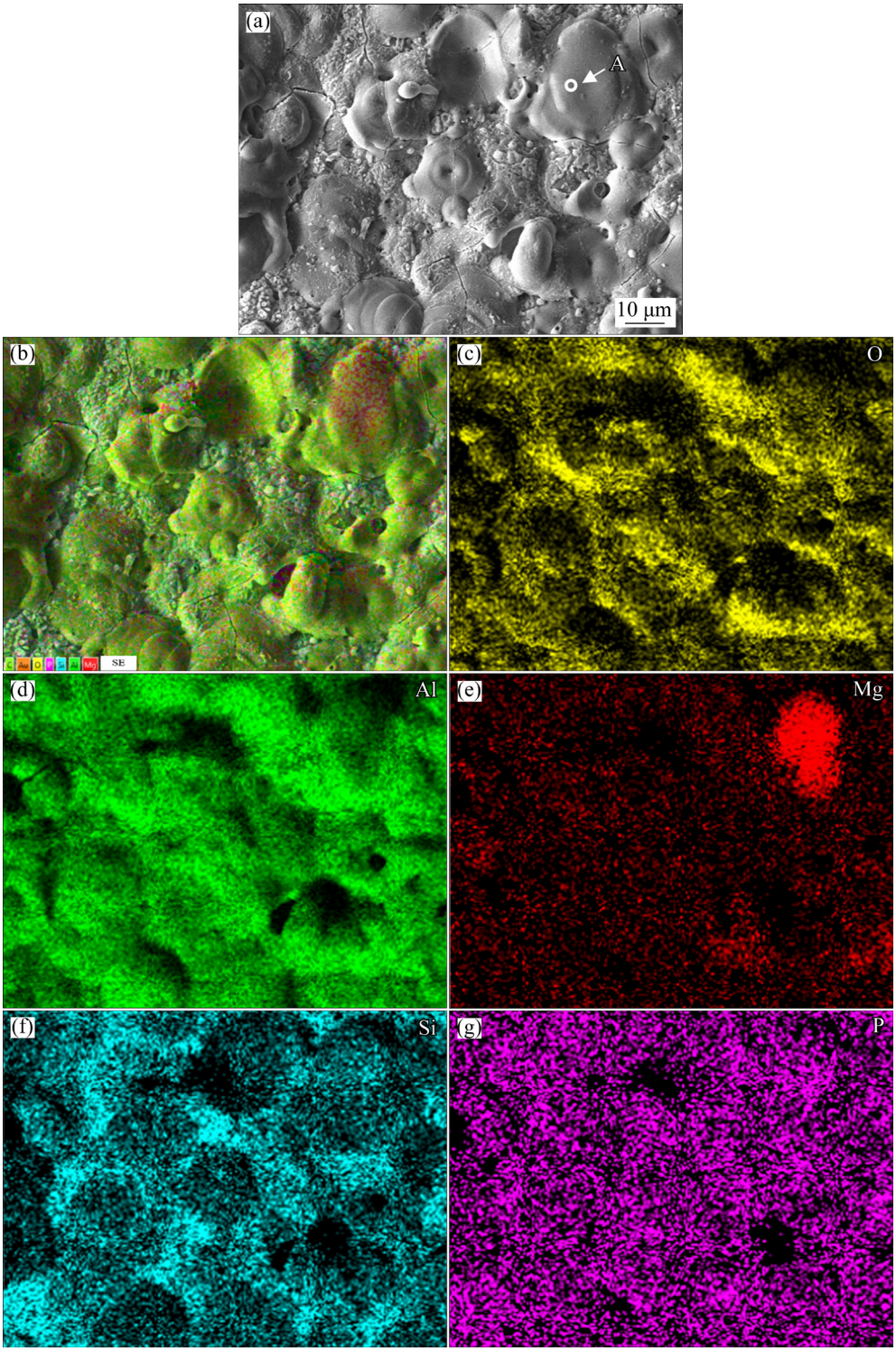

Fig. 4 Surface morphology of coating formed on Al−AZ31 magnesium alloy after 10 min PEO treatment (a) and corresponding merged image (b) and independent EDS element mappings for O (c), Al (d), Mg (e), Si (f) and P (g)

due to its low content. However, the element mapping shows that P element distributes uniformly on the surface.

Figure 5 shows the cross-sectional morphology and elemental mappings of the coating after 10 min PEO treatment. Figure 5(a) shows that the coating oxide has protruded into the AZ31 substrate at many positions as indicated by the white arrows, indicating that the magnetron sputtered Al layer at these positions has been completely consumed, and the Mg substrate begins to participate in the coating formation. As shown in Fig. 5(b), there are still

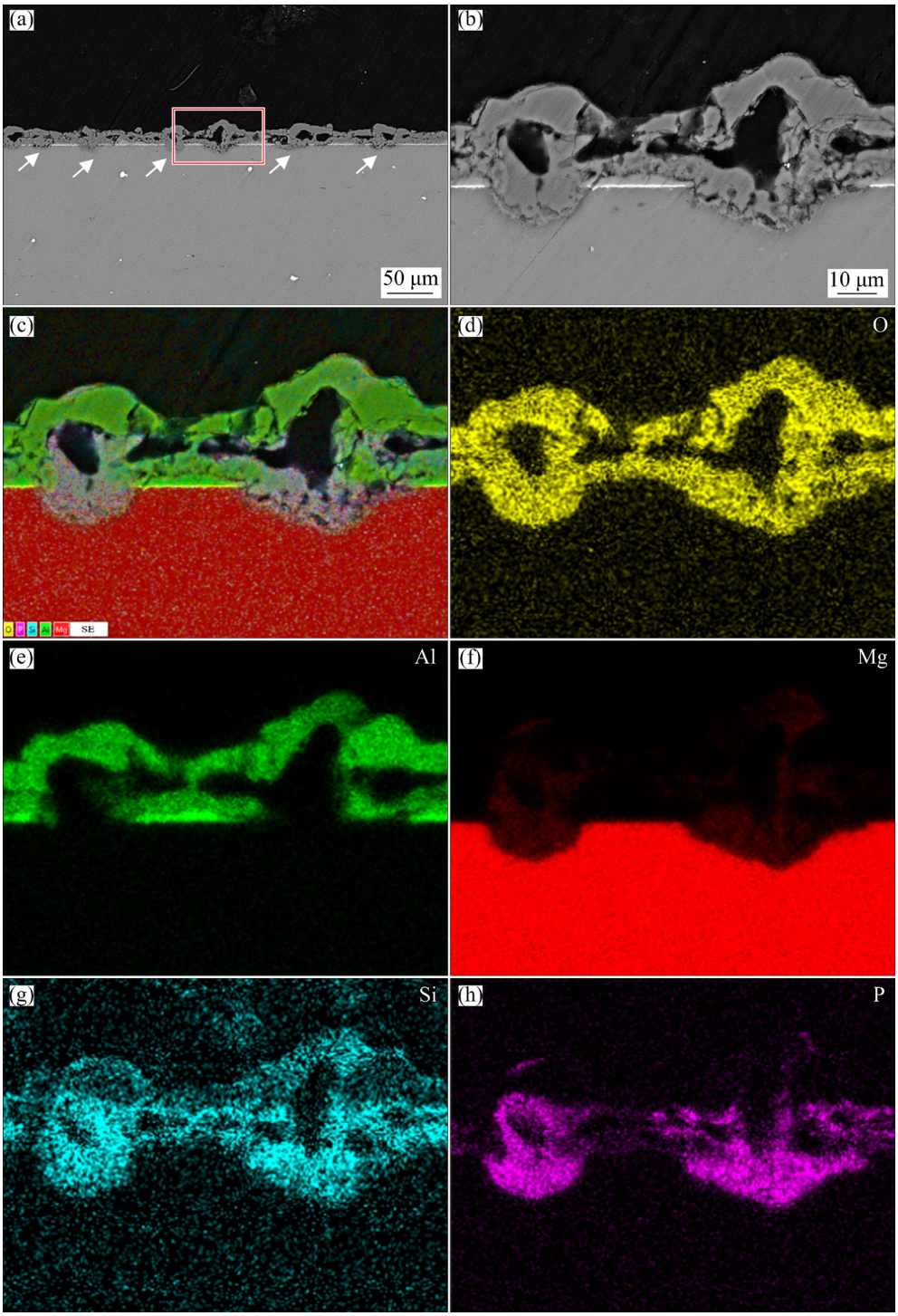

Fig. 5 Scanning electron micrographs showing cross-section of coating formed on Al−AZ31 magnesium alloy after 10 min PEO treatment (a, b) and corresponding merged image (c) and independent EDS element mappings for O (d), Al (e), Mg (f), Si (g) and P (h)

some remaining magnetron sputtered Al layers at some parts of the cross-section, which is shown in bright contrast at the oxide coating/AZ31 Mg alloy interface. The coating protrudes toward both the interfaces of electrolyte/coating and coating/substrate, indicating that coating growth mainly occurs at these locations. Between the outer and inner layers of the coating, there are two large-sized pores. This type of coating structure is often encountered in previous studies [28]. According to literatures, the big pores are associated with the gas expansion accompanied by strong plasma discharges [28,36].

The elemental mapping in Fig. 5 shows the

distribution of O, Al, Mg, Si and P elements on the cross section. The O element is evenly distributed throughout the coating. The Si element is also approximately uniformly distributed in the entire coating. P element is mainly distributed at the lower part of the coating. Al element is distributed above the original interface of Al layer/AZ31 Mg alloy. Those parts of coating that are located below the Al layer and protrude into the AZ31 substrate are evidently the newly formed PEO coatings during several latest discharge events. The absence of Al element in these lower protruding parts of the coating suggests that the previously formed alumina oxide may not have participated in the new coating formation process. Furthermore, the outer part of the coating mainly consists of the previously formed alumina, which is less affected by the latest discharge. Mapping of Mg shows that Mg is mainly distributed at the lower part of the discharge channels. Only a small amount of Mg has reached the upper part of the coating. Besides, Mg is also found within the pores and outer part of the coating.

Figure S1 (Supporting Materials) shows the cross sectional morphology and element mappings at another location of the same coating. Its elemental distribution is basically similar to that in Fig. 5. It can be clearly seen that although Mg from substrate has been consumed due to the latest plasma discharge, the Al element of the previously formed alumina oxide is still distributed at the original position of the magnetron sputtered layer. The result indicates that previously formed alumina oxide seems to have not undergone re-melting at the several latest plasma discharges.

Figure 6 shows the surface morphology and elemental mappings for the Al−AZ31 sample after

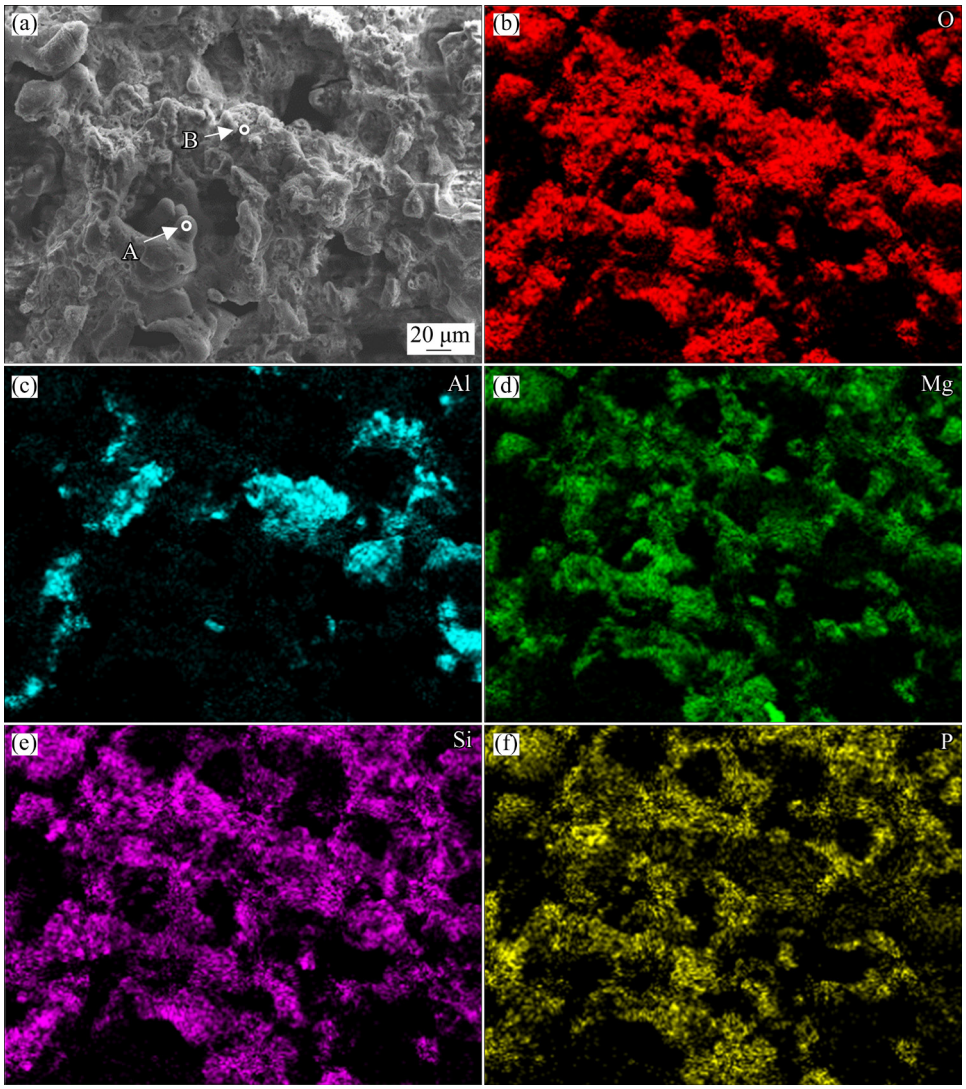

Fig. 6 Scanning electron micrograph showing surface of Al−AZ31 magnesium alloy after 60 min PEO treatment (a) and corresponding EDS element mappings for O (b), Al (c), Mg (d), Si (e) and P (f)

60 min PEO. It can be seen that the surface undulation of the coating has been significantly improved. The area indicated by Point A in the secondary electron image shows the morphology of large solidified melts, which may be formed after the repeated melting−cooling process of plasma discharges. The area at Point B shows finer features and may be the oxide formed at earlier stage. EDS analysis results of Points A and B are listed in Table 1. The results confirm the above speculation: the composition of Mg at Point A is high, reaching ~29.06 at.%, while that of Al is only ~1.1 at.%. The Al composition at Point B is 17.36 at.%, which is higher than the Mg content (12.22 at.%) at this point. The element map of Al shows island-like distribution of this element. However, the other elements of O, Mg, Si and P are relatively uniformly distributed on the whole surface. The presence of Al element in the island-like feature indicates that the previously formed alumina has not been significantly taken parted in the following coating formation process.

Table 1 EDS analysis results of positions indicated in Fig. 6

Point	Element composition/at.%						
	O	Mg	Al	Si	P	Na	Ca
A	51.44	29.06	1.09	7.83	8.14	2.43	−
B	53.66	12.22	17.36	6.28	8.62	1.63	0.23

Figure 7 shows the cross-sectional morphology of the coating formed after 60 min PEO and the corresponding elemental mappings. The low magnification image in Fig. 7(a) shows a non-uniform coating with thickness larger than 100 μm. The coating shows pores with different sizes and vertical cracks are also found. The EDS mapping shows the distribution of O, Al, Mg, Si, P, and Na in the cross section. Of all these elements, O, Mg, Si, P and Na distribute uniformly on the whole cross section. The distribution of Al is different, which is only found in a small island-like feature on the upper part of the coating. The height of the Al-enriching island is ~ 25 μm, which is close to the coating oxide thickness in Fig. 5(b). However, the continuous alumina layer formed at the early stage is interrupted at this time, owing to the repeated plasma discharges occurring at the later PEO stage.

3.4 Phase composition

The phase composition of the PEO coatings formed for different time on the Al−AZ31 samples was investigated by XRD (Fig. 8). For the coating formed for 5 min, the peaks of metallic Al and Mg from the underlying substrate appear in the XRD pattern, due to the penetration by the X-rays. γ-Al_2O_3 is the main phase composition of the coating formed for 5 min. This is consistent with the SEM results that the Al layer has not been totally consumed at this stage. For the PEO coating formed for 12 min, only the peaks of γ-Al_2O_3 are detected, and the peaks of Al and Mg disappear, indicating that the thickness of the PEO layer increases at this time. For the PEO coating formed for 60 min, the intensity of the diffraction peaks of γ-Al_2O_3 is obviously reduced, and the diffraction peaks of Mg_2SiO_4 and MgO are clearly detected in the XRD pattern. The sample coated for 60 min also suggests that there might be an amorphous phase as indicated by the broad peak between 15° and 30° (in 2θ).

3.5 Corrosion properties

During the corrosion process, the OCP is determined by the balance between the anodic and cathodic reactions on the electrode surface. Therefore, the change of the OCP of the specimen can give some information about the corrosion process.

Figure 9 shows the results of the OCP and potentiodynamic polarization curve tested in 3.5 wt.% NaCl for the AZ31 magnesium alloy, the magnetron sputtered Al−AZ31 samples before and after PEO treatments. In Fig. 9(a), the OCP of Al-coated AZ31 alloy is the most positive within 1 h immersion. The OCP first increases gradually with the prolongation of the immersion time, reaching −0.558 V at 1073 s. However, sawtooth-like fluctuations are often observed during the evolution of OCP. The fluctuation is featured by a sudden drop and then recovers gradually to positive direction. This phenomenon may be related to the pitting nucleation on the surface of the aluminum coating and its repair process [37]. When the immersion time reaches 3100 s, the OCP drops continuously to a more negative value of −1.464 V at 3362 s; after that the OCP recovers to the positive direction to a small extent and decreases again. This fast decrease of the OCP to more negative values

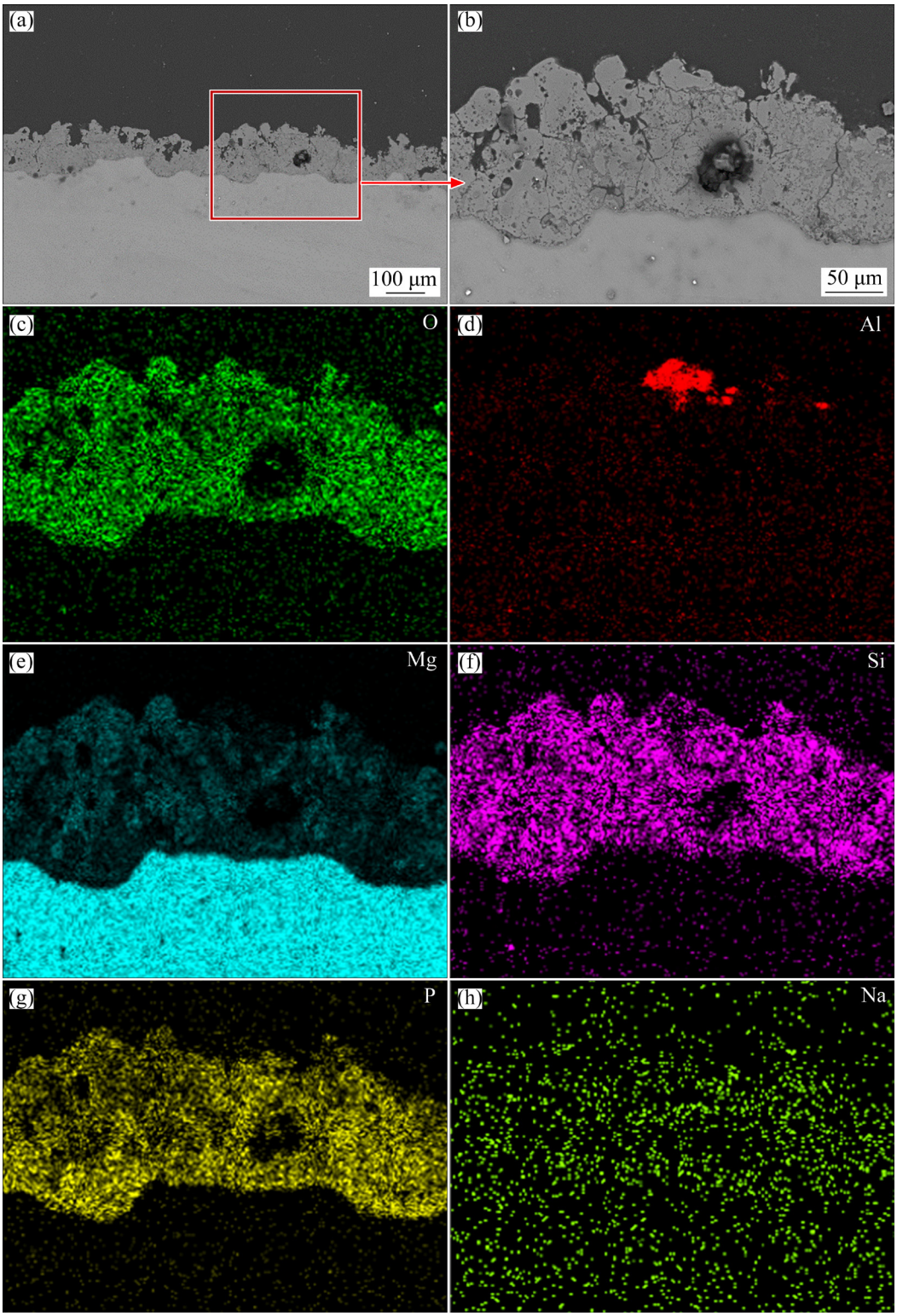

Fig. 7 Scanning electron micrographs showing cross section of coating formed after 60 min PEO on Al−AZ31 magnesium alloy (a, b) and EDS elemental mappings corresponding to O (c), Al (d), Mg (e), Si (f), P (g) and Na (h)

may be related to the fact that the corrosive solution has reached the interface of the Al/AZ31magnesium alloy, which has also been observed in Ref. [12]. However, the potential drop occurred at earlier immersion times (18−108 s) in Ref. [12]. The delayed transition indicates that the corrosion resistance of the present magnetron sputtered layer is better than that in Ref. [12], which can be attributed to the fact that a denser Al layer with finer grains retards the ingress of corrosive species.

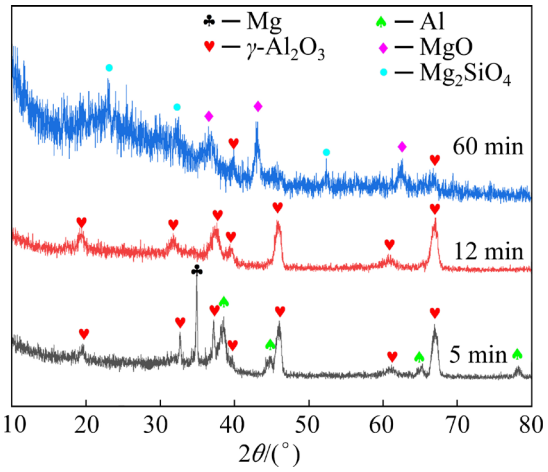

Fig. 8 XRD patterns for Al−AZ31 magnesium alloy duplex system after PEO treatment for 5, 12 and 60 min

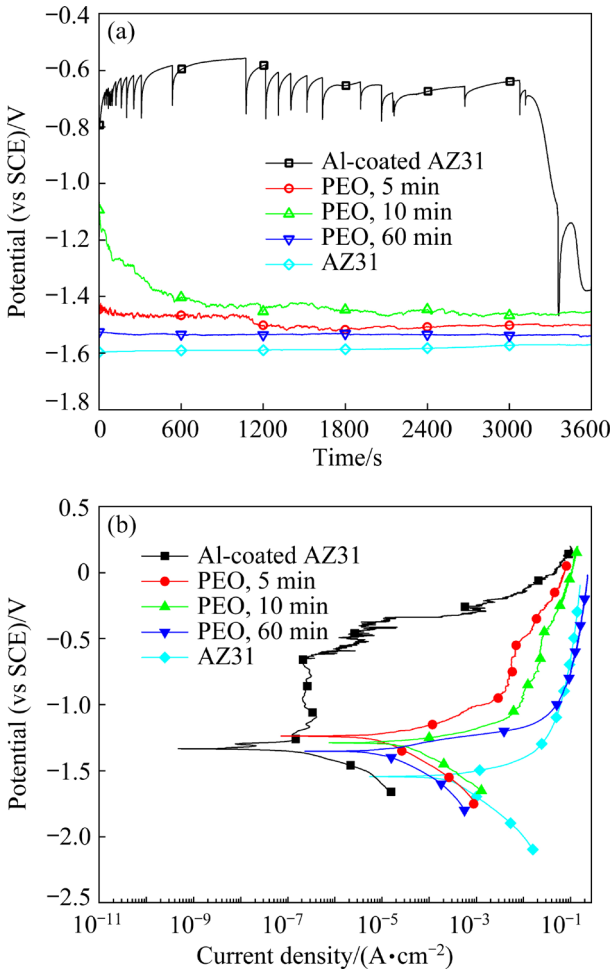

Fig. 9 Open circuit potential (a) and potentiodynamic polarization curves (b) recorded in 3.5 wt.% NaCl solution for untreated AZ31 magnesium alloy, Al-coated AZ31 magnesium alloy, and Al-coated samples after PEO treatment for 5, 10 and 60 min

All the PEO coatings show more negative OCP values than the sample coated with Al only (Fig. 9(a)). For the sample with 10 min PEO treatment, the initial OCP is −1.094 V, which then decreases continuously to about −1.4 V at 600 s, after that OCP is relatively stable, with a final value of −1.453 V at 3600 s. The variation of OCP of PEO samples treated for 5 and 60 min is similar to that of the sample treated for 10 min, but their OCP values are more negative. The OCP of the untreated AZ31 alloy is the most negative, which is basically maintained at around −1.600 V throughout the immersion time.

Figure 9(b) shows the polarization curves of the samples. Compared with that of AZ31 magnesium alloy, the polarization curve of the alloy coated with the Al layer is shifted to the direction of lower current densities, indicating a significantly improved corrosion resistance. The Al−AZ31 magnesium alloy also shows a passivation section between −1.25 and −0.645 V in the anodic branch of the polarization curve, and the current density of passivation is about 2.4×10^{-7} A·cm^{-2}. This value is about 3 orders smaller than that of the magnetron sputtered Al layer in Ref. [12]. A pitting potential of −0.645 V is detected for the Al coated sample, after which the anodic current density increases significantly.

In contrast, the AZ31 magnesium alloy and the PEO-treated Al−AZ31 samples do not show the behavior of passivation. The corrosion potential, current density and also the anodic (b_a) and cathodic (b_c) Tafel slopes of each sample are listed in Table 2. The corrosion current densities are obtained by the Tafel extrapolation method. It can be seen that the Al−AZ31 magnesium alloy shows

Table 2 Corrosion parameters derived from polarization curves in Fig. 9(b)

Sample	J_{corr}/(A·cm^{-2})	φ_{corr}(vs SCE)/V	b_a/(mV·dec^{-1})	b_c/(mV·dec^{-1})
AZ31	2.54×10^{-4}	−1.54	156	248
Al-coated AZ31	1.43×10^{-7}	−1.33	319	106
PEO, 5 min	3.93×10^{-6}	−1.25	186	181
PEO, 10 min	3.61×10^{-5}	−1.30	109	186
PEO, 60 min	5.52×10^{-6}	−1.35	96	187

the least corrosion current density, while the PEO treatment has increased the corrosion current density of the samples; however, their values are lower than the value of the untreated AZ31 alloy.

EIS was used widely to evaluate the corrosion behavior of PEO coatings [38]. EIS data of the Al-coated AZ31 alloy and the PEO coatings formed for different time were recorded in 3.5 wt.% NaCl solution at the immersion time of 1, 3 and 5 h, respectively. Figure 10 shows the Nyquist and Bode plots of the EIS results. At the immersion time of 1 h, the Al-coated sample shows the largest depressed semicircle in the Nyquist plots, followed by the PEO coating formed for 60 min. The smallest semicircles are observed with the Nyquist plots of the coatings formed for 5 and 10 min, and the Nyquist plots of these coatings are composed of more than one depressed capacitive semicircle. The Bode phase angle plot of the Al-coated sample shows almost constant phase angle at about −80° over a wide frequency range (1−1000 Hz), which suggests the presence of highly stable passive film [39]. Moreover, the broad phase angle may indicate that it actually consists of two overlap time constants. The PEO treatments have caused significant changes in the Bode phase angle plots.

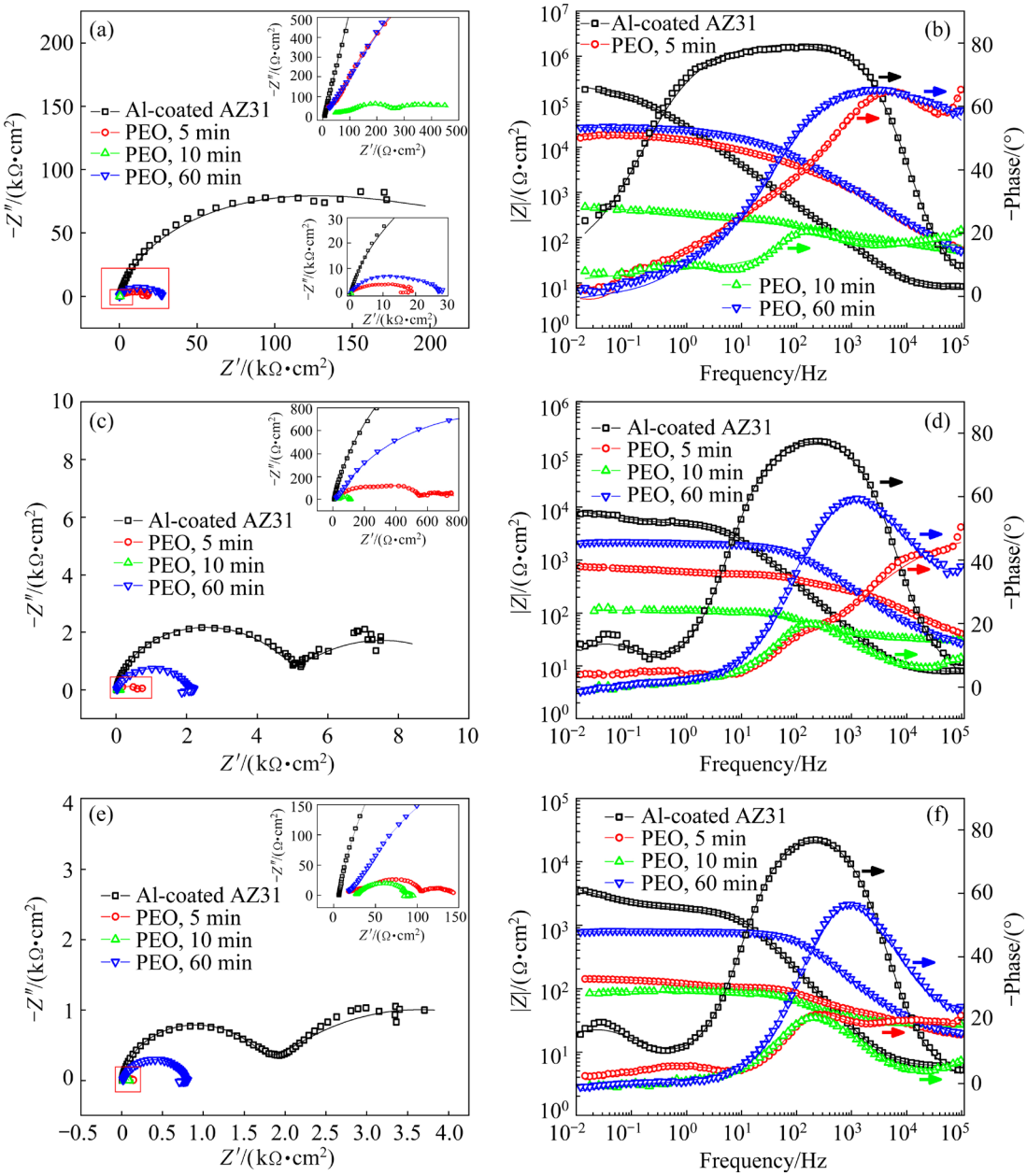

Fig. 10 EIS spectra recorded after being immersed in 3.5 wt.% NaCl solution for 1 h (a, b), 3 h (c, d) and 5 h (e, f), for Al-coated AZ31 magnesium alloy and PEO coatings formed for different time

All the PEO coatings show lower maximum phase angle values. Compared with the Al-coated AZ31 sample, the PEO coatings show higher impedance values at the high frequency domain in the Bode modulus plots, which may be attributed to the fact that high frequency impedance usually reflects the resistance of the PEO coatings [39]. However, the Al-coated AZ31 magnesium alloy shows the highest impedance modulus at the low frequency domain.

At the extended immersion time of 3 and 5 h, two distinctive depressed semicircles are more obvious in the Nyquist plots of the Al-coated AZ31 magnesium alloy. For the PEO coating formed for 60 min, an additional inductive loop is observed at the low frequency domain of the Nyquist plots at 3 and 5 h. The presence of inductive loop is a common phenomenon for Mg and its alloys, which is believed to be associated with pitting corrosion [40−43]. In EIS spectra recorded at the same immersion time, the low-frequency impedance modulus of the Al-coated AZ31 sample is always higher than that of the PEO-treated samples. This result shows that PEO treatment in the sodium silicate-sodium hexametaphosphate electrolyte could not improve the corrosion resistance of the magnetron sputtering layer, which is consistent with the results of the polarization curves. It is also observed in Fig. 10 that the low-frequency impedance modulus of the same sample decreases with the prolongation of immersion time. The reduction in the diameter of the capacitive semicircle, the change in the position of the maximum phase angle, and the reduction in the impedance modulus mean that the structure of the PEO coating may be changed. In the low frequency region, the magnitude of the impedance modulus shows the regularity at different immersion time: Al-coated AZ31 > PEO, 60 min > PEO, 5 min > PEO, 10 min. This order is similar to that obtained from the polarization curves. The only difference is that polarization curves indicate a better corrosion resistance of the PEO, 5 min sample than that of the PEO, 60 min sample.

Owing to the characteristics of the EIS spectra, different electrical equivalent circuits (EECs) are used to fit the EIS spectra. Figure 11 presents the EECs and Table 3 lists the fitted parameters. The solid lines in Fig. 10 represent the fitted results, which match well with the original data points.

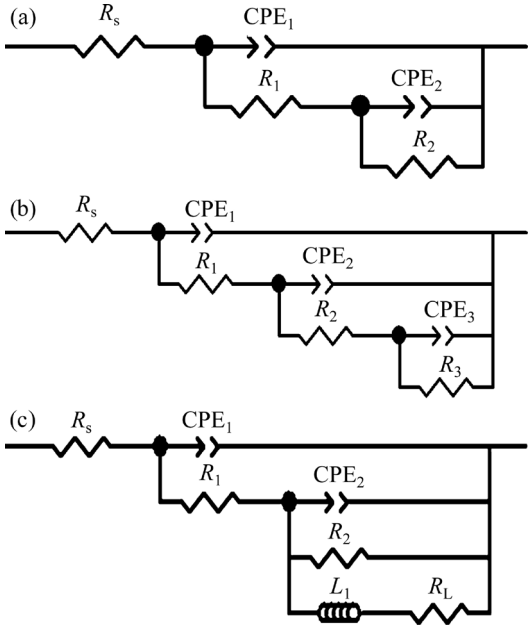

Fig. 11 Electrical equivalent circuits used for fitting EIS spectra recorded at different stages for different samples in Fig. 9: (a) Al-coated AZ31Mg alloy (immersion for 1, 3 and 5 h), PEO, 10 min coating (immersion for 1, 3 and 5 h), and PEO, 60 min coating (immersion for 1 h); (b) PEO, 5 min coating (immersion for 1, 3 and 5 h); (c) PEO, 60 min coating (immersion for 3 and 5 h)

The chi-square values (χ^2) between 0.6×10^{-3} and 3.1×10^{-3} in Table 3 also indicate good fitting. The EEC in Fig. 11(a) is used for fitting the EIS spectra of the Al-coated AZ31 magnesium alloy, PEO, 10 min sample after immersion for 1, 3 and 5 h and the PEO, 60 min sample after 1 h immersion. In this EEC, R_s is the solution resistance; R_1 and CPE_1 represent the resistance and capacitance of the magnetron sputtered Al layer or the PEO coatings formed for 10 and 60 min, respectively; R_2 and CPE_2 represent the charge transfer resistance and double-layer capacitance, respectively, of the interface between the magnetron sputtered Al layer and the AZ31 magnesium alloy or the interface between the PEO coatings and the AZ31 magnesium alloy substrate. In electrochemistry, constant phase elements (CPE) are commonly used to represent the non-ideal capacitance behavior caused possibly by the effect of surface roughness [44].

The EIS spectra of the PEO, 5 min sample consists of three time constants; therefore, the ECC in Fig. 11(b) is used for fitting its EIS spectra at different immersion time. R_s is the solution resistance; R_1 and CPE_1 represent the resistance and

Table 3 Fitted equivalent circuit parameters for EIS spectra in Fig. 10

Sample	Immersion time/h	R_s/ ($\Omega\cdot cm^2$)	CPE_1/ ($s^{-n}\cdot\Omega^{-1}\cdot cm^{-2}$)	n_1	R_1/ ($\Omega\cdot cm^2$)	CPE_2/ ($s^{-n}\cdot\Omega^{-1}\cdot cm^{-2}$)	n_2	R_2/ ($\Omega\cdot cm^2$)
Al-coated AZ31	1	8.6	4.69×10^{-6}	0.24	5970	5.86×10^{-6}	0.90	5.27×10^{5}
	3	9.2	8.01×10^{-6}	0.91	4970	8.88×10^{-5}	0.71	5.31×10^{3}
	5	6.1	1.29×10^{-5}	0.8	1734	1.56×10^{-3}	0.80	3.86×10^{3}
PEO, 5 min	1	4.5	1.11×10^{-7}	0.99	48.7	6.38×10^{-6}	0.73	127.4
	3	4.8	5.15×10^{-5}	0.58	81.7	1.62×10^{-5}	0.96	84.7
	5	3.2	1.73×10^{-4}	0.59	43.2	2.66×10^{-5}	0.83	26.0
PEO, 10 min	1	45.0	1.40×10^{-3}	0.80	647.8	3.39×10^{-3}	0.99	77.5
	3	20.7	1.58×10^{-4}	0.31	39.0	9.01×10^{-5}	0.76	75.8
	5	18.1	1.69×10^{-4}	0.77	27.9	1.16×10^{-4}	0.76	62.1
PEO, 60 min	1	25.8	1.26×10^{-6}	0.74	20421	2.16×10^{-5}	0.78	6.8×10^{3}
	3	28.9	3.19×10^{-7}	0.87	35.4	3.30×10^{-6}	0.77	2.1×10^{3}
	5	25.9	1.25×10^{-7}	0.85	22.6	4.18×10^{-6}	0.82	761.8

Sample	Immersion time/h	CPE_3/ ($s^{-n}\cdot\Omega^{-1}\cdot cm^{-2}$)	n_3	R_3/ ($\Omega\cdot cm^2$)	L_1/ ($H\cdot cm^{-2}$)	R_L/ ($\Omega\cdot cm^2$)	$\chi^2/10^{-3}$
Al-coated AZ31	1	−	−	−	−	−	1.1
	3	−	−	−	−	−	1.3
	5	−	−	−	−	−	0.6
PEO, 5 min	1	3.73×10^{-4}	0.80	134.2	−	−	3.1
	3	0.016	0.59	51.5	−	−	0.6
	5	0.035	0.93	6.2	−	−	1.6
PEO, 10 min	1	−	−	−	−	−	1.0
	3	−	−	−	−	−	0.9
	5	−	−	−	−	−	0.8
PEO, 60 min	1	−	−	−	−	−	1.4
	3	−	−	−	4.66×10^{5}	2.1×10^{4}	0.6
	5	−	−	−	1.48×10^{5}	8.8×10^{3}	0.6

capacitance, respectively, of the PEO coating; R_2 and CPE_2 represent the resistance and capacitance of the remaining magnetron sputtered Al layer; R_3 and CPE_3 represent the charge transfer resistance and double layer capacitance respectively, at the interface between the magnetron sputtered Al layer and the magnesium alloy.

The ECC in Fig. 11(c) is used for fitting the EIS spectra of the PEO, 60 min coating after immersion for 3 and 5 h. In this equivalent circuit, R_s is the solution resistance; R_1 and CPE_1 represent the resistance and capacitance of the PEO coating, respectively; R_2 and CPE_2 represent the charge transfer resistance and double-layer capacitance at the interface between the PEO coating and the AZ31 magnesium alloy substrate; R_L and L_1 are parameters associated with the inductive loop caused by pitting of the Mg alloy.

According to the fitted results in Table 3, the magnetron sputtered layer alone can provide sufficient corrosion protection to the magnesium alloy substrate, as the highest impedance value is recorded during the whole immersion process. The charge transfer resistances after 5 h immersion are 3860, 26.0, 62.1 and 761.8 $\Omega\cdot cm^2$ for the Al-coated AZ31 magnesium alloy, PEO, 5 min coating, PEO, 10 min coating, and PEO, 60 min coating, respectively. The results indicate that the PEO

coatings formed for 5 and 10 min have much higher corrosion rates compared with the other two.

4 Discussion

4.1 Structure of discharge channels

By tracing the distribution of different elements in the PEO coatings after the Al layer is consumed, some new information about the structure of discharge channels is obtained, which is presented in the schematic illustration in Fig. 12. According to Ref. [28], very strong localized anodic current densities exist within the discharge channels. Therefore, the Joule heat generated within a discharge channel will lead to the melting of part of the material in the discharge channel and the generation of plasma. However, according to the present study, the previously formed oxide materials, such as MgO and Al_2O_3, are largely not subjected to re-melting within the discharge channels during the subsequent discharge events.

According to a handbook [45], the melting points of Al_2O_3 and MgO are 2054 and 2825 °C, respectively. However, the melting points of the metals corresponding to these oxides are significantly lower, i.e. 650 °C for Mg, and 660 °C for Al [45], respectively. Therefore, at the lower part of active plasma discharge channel, a small amount of the metal from the substrate is considered to be preferentially melted, due to low melting point of the substrate metal. Afterwards, the molten metal reacts violently with electrolyte species to form oxides. The reactions of MgO and Al_2O_3 formation are exothermic, releasing large amount heat, which helps to keep the newly formed oxides in a molten state. However, the previously formed oxides, for example, those oxides located at the upper part of the discharge channel, are less affected by the high temperature discharges due to their extremely high melting point, and they can remain in solid state during the plasma discharging process. The presence of the solid state oxides in the upper part of the discharge channels hinders the mass transfer process within the discharge channels. However, due to the porosity of the oxide coating, a small amount of the molten oxides can still reach the surface of the oxide coating through the micropores and defects (see Fig. 12(b)). In the PEO process, elements from electrolyte, such as O, Si, and P, exist in the form of anions, so they can easily reach the coating/substrate interface along with the electrolyte through the micropores of the coating to participate in the coating formation. Therefore, when the PEO coating reaches a certain thickness, coating oxides are mainly formed at frontiers of the discharge channels, with newly formed oxides protruding into the metal substrate. This type of coating formation explains the phenomenon that the interface between PEO coatings and substrate metal is usually wavy, as can be found in Refs. [28,46,47]. After new oxide material is formed at the particular positions (discharge areas), the resistance at these locations increases significantly, and subsequent plasma discharges occur in other locations on the coating. These processes are repeated during the whole PEO duration, and finally, thick coatings are formed toward the substrate.

The model presented in Fig. 12 is consistent with the study of others. In the work of GAO et al [30], an aluminized Al layer of 60 μm was coated

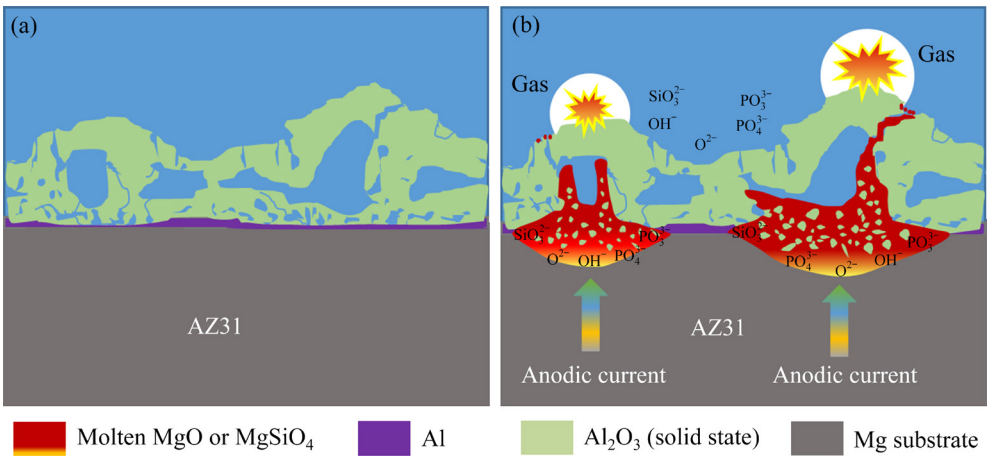

Fig. 12 Schematic illustration of later stage coating formation process on Al−AZ31 duplex system before (a) and after (b) plasma discharges

on Ti substrate and the sample was then subjected to PEO treatment. They found that, after the consumption of Al layer, the lower part of discharge channels also extended into the Ti substrate, which implied the melting of Ti at the coating/substrate interface. Hence, it was proposed that discharge channel consists of a groove-like oxidation region at coating/substrate interface [30]. It should be pointed out that the present model is mainly based on PEO at the relatively early stage of 10 min. Because the Al layer has been consumed completely at later stage of PEO, it is difficult to trace the coating formation mechanism at the time of 60 min. However, the mechanism is not changed much at the later stages. MATYKINA et al [48] investigated the PEO coating formation mechanism by ^{18}O tracer. After the formation of ~70 μm-thick coating in the electrolyte prepared by conventional water, the coating was transferred into the ^{18}O containing electrolyte for another 5 min PEO treatment. Subsequent examination showed that the ^{18}O ion species is mainly distributed in a layer of coating directly adjacent to aluminium substrate. Therefore, it was concluded that fresh alumina is formed within the coating material near to the substrate [48].

This study contributes to our further understanding of the PEO discharge process. First of all, it is clear that although the temperature of a discharge channel is very high, most of the previously formed oxides within the discharge channel, especially the oxides located at the coating outer layer, are kept in solid state. In contrast, molten oxides are mainly formed at the lower part of a discharge channel. These molten oxides are formed by melting the substrate metal. Therefore, new oxides are formed at the front of the discharge channels close to the substrate. Although a small fraction of the molten oxides of the base metal can flow out to the surface of the coating, this is not the dominant coating formation mechanism. The interconnected pores may provide the passages for the flowing out of the molten oxides. However, the previously formed oxides at the discharge channels block most of the formed molten oxides. Therefore, the mechanism by direct injection of molten oxide does not play an important role in PEO coating formation.

During the formation of PEO coatings, the movement of anions to interfaces of the coating/substrate in the high electric field also plays an important role. The migration of these anionic species is most probably carried out through the micropores of the PEO layer. During the PEO process, the micropores in the coating are likely filled with electrolyte.

4.2 Corrosion mechanism

The present study shows that the magnetron sputtered Al layer can provide good corrosion protection for the substrate. However, poor corrosion resistance was found with a magnetron sputtered Al layer on AZ31 magnesium alloy in a previous study [12]. The reason for the lower corrosion resistance can be attributed to the lower quality of the magnetron sputtered layer. The layer in Ref. [12] was deposited with an excessively fast deposition rate and the grain size of the layer is coarser than that of the Al layer in the present study. As a result, the negative shift of OCP occurs at a much delayed immersion time in this study. In addition, the polarization curve also shows that the corrosion current density of the magnetron sputtered layer in this study is about 2.8×10^{-7} A·cm^{-2}, which is nearly three-order lower than that of the Al layer in Ref. [12].

In this study, PEO treatment does not improve the corrosion resistance of the magnetron sputtered layer. This phenomenon may be caused by the excellent corrosion resistance of the magnetron sputtered Al layer itself, while the PEO layer is porous and cannot completely hinder the intrusion of corrosive media. As the PEO treatment consumes a part of the Al layer, the corrosion resistance of the sample after PEO treatment is decreased, so the sample after 5 min PEO treatment has higher corrosion resistance than the sample treated with 10 min PEO treatment. However, the slightly improved corrosion resistance of the sample treated for 60 min PEO is caused by the much increased thickness of the sample. Of course, it must be pointed out that the corrosion resistance of PEO coatings is related to the types of the electrolytes. In previous study, the Al−AZ31 magnesium alloy duplex system was treated with aluminate and silicate electrolytes, respectively, and the corrosion resistance of the resultant coating in aluminate is higher than that of the coating prepared in silicate.

Although the subsequent PEO treatment does not improve corrosion resistance of the Al−coated

AZ31 magnesium alloy in this study, it must be noted that thicker and harder oxide layers can be formed on the magnetron sputtered layer, which is significantly important for improving the wear resistance of the sample [12].

5 Conclusions

(1) Strong local current melts the substrate metal at the frontier of a discharge channel, which then reacts with electrolyte species to form molten oxides.

(2) New coating oxides are mainly formed at the frontier of the discharge channels, with protrusions up to tens of microns into the magnesium alloy substrate. These protrusions may be the result of repeated plasma discharges.

(3) The high temperature discharges do not affect too much the previously formed oxides in the upper coating, which are largely kept in solid state and at their original positions.

(4) Only a small amount of the oxides of the substrate metal can flow out through the micropores to reach the top coating. The micropores also support the free access of the electrolyte species to the innermost of coatings.

(5) The magnetron sputtering Al layer can provide excellent corrosion protection to the magnesium alloy, and the subsequent PEO treatment in the electrolyte cannot further improve the corrosion resistance of the alloy.

CRediT authorship contribution statement

Pan-feng HU: Investigation, Validation, Visualization, Writing − Original draft; **Bing-jian WEI:** Investigation, Visualization; **Yu-lin CHENG:** Investigation, Visualization; **Ying-liang CHENG:** Conceptualization, Project administration, Validation, Writing − Review and editing.

Declaration of competing interest

The authors declare that they have no known competing financial interests or personal relationships that could have appeared to influence the work reported in this paper.

Acknowledgments

This work is supported by the National Natural Science Foundation of China (No. 51671084).

Supporting Materials

Supporting Materials in this paper can be found at: http://tnmsc.csu.edu.cn/download/09-p0139-2022-0756-Supporting_Materials.pdf.

References

[1] LUO A A. Magnesium: Current and potential automotive applications [J]. Journal of the Minerals Metals & Materials Society, 2002, 54: 42−48.

[2] MORDIKE B, EBERT T. Magnesium: Properties−applications−potential [J]. Materials Science and Engineering A, 2001, 302: 37−45.

[3] YANG Ming-bo, PAN Fu-sheng, ZHANG Jing, ZHANG Jin. An analysis of the development and applications of current and new Mg−Al based elevated temperature magnesium alloys [J]. Materials Science Forum, 2005, 488: 923−926.

[4] HUSSEIN R, NORTHWOOD D, SU J F, NIE X. A study of the interactive effects of hybrid current modes on the tribological properties of a PEO (plasma electrolytic oxidation) coated AM60B Mg-alloy [J]. Surface and Coatings Technology, 2013, 215: 421−430.

[5] DAROONPARVAR M, YAJID M A M, YUSOF N M, BAKHSHESHI-RAD H R. Preparation and corrosion resistance of a nanocomposite plasma electrolytic oxidation coating on Mg−1%Ca alloy formed in aluminate electrolyte containing titania nano-additives [J]. Journal of Alloys and Compounds, 2016, 688: 841−857.

[6] WALSH F C, LOW C T J, WOOD R J K, STEVENS K T, ARCHER J, POETON A R, RYDER A. Plasma electrolytic oxidation (PEO) for production of anodised coatings on lightweight metal (Al, Mg, Ti) alloys [J]. Transactions of the Institute of Metal Finishing, 2009, 87: 122−135.

[7] ARNELL R, KELLY P, BRADLLEY J. Recent developments in pulsed magnetron sputtering [J]. Surface and Coatings Technology, 2004, 188/189: 158−163.

[8] DENG Q L, SUN K K, ZHOU G C, SONG J L, WANG Y, HU D J. Research on surface quality control of moulds formed by plasma arc spraying [J]. Advances in Materials Manufacturing Science and Technology, 2004, 620: 471−472.

[9] HUNG Jung-chou, LIU Yi-ren, TSUI H P, FAN Zhi-wen. Electrode insulation layer for electrochemical machining fabricated through hot-dip aluminizing and microarc oxidation on a stainless-steel substrate [J]. Surface and Coatings Technology, 2019, 378: 124995.

[10] HE Xiao-rui, FENG Tian, CHENG Yu-lin, HU Pan-feng, LE Zheng-zhou, LIU Zi-hua CHENG Ying-liang. Fast formation of a black inner α-Al_2O_3 layer doped with CuO on Al−Cu−Li alloy by soft sparking PEO process [J]. Journal of the American Ceramic Society, 2023, 106: 7019−7042.

[11] ZHU Mao-dong, ZHANG Dong-ping, JIANG Shu-yun, LIU Shu-guang, QI Hong-ji, YANG Yu. Phase evolution and thermochromism of vanadium oxide thin films grown at low substrate temperatures during magnetron sputtering [J]. Ceramics International, 2021, 47: 15491−15499.

[12] WEI Bing-jian, CHENG Yu-lin, LIU Yuan-yuan, ZHU Zhun-da, CHENG Ying-liang. Corrosion and wear resistance of AZ31 Mg alloy treated by duplex process of magnetron sputtering and plasma electrolytic oxidation [J]. Transactions of Nonferrous Metals Society of China, 2021, 31: 2287−2306.

[13] CHENG Ying-liang, FENG Tian, CHENG Yu-lin. A systematic study of the role of cathodic polarization and new findings on the soft sparking phenomenon from plasma electrolytic oxidation of an Al−Cu−Li alloy [J]. Journal of the Electrochemical Society, 2022, 169: 071505.

[14] CHENG Yu-lin, XIE Huan-jun, CAO Jin-hui, CHENG Ying-liang. Effect of NaOH on plasma electrolytic oxidation of A356 aluminium alloy in moderately concentrated aluminate electrolyte [J]. Transactions of Nonferrous Metals Society of China, 2021, 31: 3677−3690.

[15] DAVOODI F, ATAPOUR M, BLAWERT C, ZHELUDKEVICH M. Wear and corrosion behavior of clay containing coating on AM 50 magnesium alloy produced by aluminate-based plasma electrolytic oxidation [J]. Transactions of Nonferrous Metals Society of China, 2021, 31: 3719−3738.

[16] WANG Xiao-ming, ZHANG Fu-qin. Influence of anions in phosphate and tetraborate electrolytes on growth kinetics of microarc oxidation coatings on Ti6Al4V alloy [J]. Transactions of Nonferrous Metals Society of China, 2022, 32: 2243−2252.

[17] ZHONG Sheng, LI Guo-qiang, ZHANG Shu-fang, ZHAO Rong-fang, JIANG Xiong-ying, ZHANG Rong-fa. Preparation and formation mechanism of anodic coatings co-doped with Ga, Si, and P ions on Ti−6Al−4V alloys [J]. Materials Chemistry and Physics, 2022, 282: 125923.

[18] QIN J, SHI X T, LI H Y, ZHAO R F, LI G Q, ZHANG S F, DING L Y, CUI X J, ZHAO Y, ZHANG R F. Performance and failure process of green recycling solutions for preparing high degradation resistance coating on biomedical magnesium alloys [J]. Green Chemistry, 2022, 24: 8113−8130.

[19] LV Jia-hui, CHENG Ying-liang. Amorphous coatings on tantalum formed by plasma electrolytic oxidation in aluminate electrolyte and high temperature crystallization treatment [J]. Surface and Coatings Technology, 2022, 434: 128171.

[20] CHENG Yu-lin, FENG Tian, LV Jia-hui, HU Pan-feng, CHENG Ying-liang. Plasma electrolytic oxidation of brass in aluminate electrolyte containing NaH_2PO_4 or Na_2SiO_3 [J]. Transactions of Nonferrous Metals Society of China, 2022, 32: 3985−3997.

[21] SRINIVASAN P B, LIANG Jun, BLAWERT C, DIETZEL W. Dry sliding wear behaviour of magnesium oxide and zirconium oxide plasma electrolytic oxidation coated magnesium alloy [J]. Applied Surface Science, 2010, 256: 3265−3273.

[22] ARRABAL R, MATYKINA E, HASHIMOTO T, SKELDON P, THOMPSON G. Characterization of AC PEO coatings on magnesium alloys [J]. Surface and Coatings Technology, 2009, 203: 2207−2220.

[23] CHENG Ying-liang, WANG Ting, LI Shao-xian, CHENG Yu-lin, CAO Jin-hui, XIE Huan-jun. The effects of anion deposition and negative pulse on the behaviours of plasma electrolytic oxidation (PEO)—A systematic study of the PEO of a Zirlo alloy in aluminate electrolytes [J]. Electrochimica Acta, 2017, 225: 47−68.

[24] DUNLEAVY C S, GOLOSNOY I O, CURRAN J A, CLYNE T W. Characterisation of discharge events during plasma electrolytic oxidation [J]. Surface and Coatings Technology, 2009, 203: 3410−3419.

[25] CHENG Yu-lin, ZHU Zhun-da, ZHANG Qing-he, ZHUANG Xiu-juan, CHENG Ying-liang. Plasma electrolytic oxidation of brass [J]. Surface and Coatings Technology, 2020, 385: 125366.

[26] SONG Ying-wei, DONG Kai-hui, SHAN Da-yong, HAN En-hou. Study of the formation process of titanium oxides containing micro arc oxidation film on Mg alloys [J]. Applied Surface Science, 2014, 314: 888−895.

[27] CHENG Yu-lin, WEI Bin-jian, LIU Yuan-yuan, CHENG Ying-liang. Plasma electrolytic oxidation of copper in an aluminate based electrolyte with the respective additives of Na_3PO_4, NaH_2PO_4 and NaH_2PO_2 [J]. Applied Surface Science, 2021, 565: 150477.

[28] TU Wen-bin, CHENG Yu-lin, WANG Xin-yao, ZHAN Ting-yan, HAN Jun-xiang, CHENG Ying-liang. Plasma electrolytic oxidation of AZ31 magnesium alloy in aluminate−tungstate electrolytes and the coating formation mechanism [J]. Journal of Alloys and Compounds, 2017, 725: 199−216.

[29] SUNDARARAJAN G, RAMA KRISHNA L. Mechanisms underlying the formation of thick alumina coatings through the MAO coating technology [J]. Surface and Coatings Technology, 2003, 167: 269−277.

[30] GAO Fang-yuan, HAO Li, LI Guang, XIA Yuan. The plasma electrolytic oxidation micro-discharge channel model and its microstructure characteristic based on Ti tracer [J]. Applied Surface Science, 2018, 431: 13−16.

[31] NOMINE A, TROUGHTON S C, NOMINE A V, HENRION G, CLYNE T W. High speed video evidence for localised discharge cascades during plasma electrolytic oxidation [J]. Surface and Coatings Technology, 2015, 269: 125−130.

[32] TROUGHTON S C, NOMINE A, NOMINE A V, HENRION G, CLYNE T W. Synchronised electrical monitoring and high speed video of bubble growth associated with individual discharges during plasma electrolytic oxidation [J]. Applied Surface Science, 2015, 359: 405−411.

[33] STOJADINOVIC S, JOVOVIC J, PETKOVIC M, VASILIC R, KONJEVIC N. Spectroscopic and real-time imaging investigation of tantalum plasma electrolytic oxidation (PEO) [J]. Surface and Coatings Technology, 2011, 205: 5406−5413.

[34] KANG S H, TU W B, HAN J X, LI Z, CHENG Y L. A significant improvement of the wear resistance of Ti6Al4V alloy by a combined method of magnetron sputtering and plasma electrolytic oxidation (PEO) [J]. Surface and Coatings Technology, 2019, 358: 879−890.

[35] YU L, CAO J H, CHENG Y L. An improvement of the wear and corrosion resistances of AZ31 magnesium alloy by plasma electrolytic oxidation in a silicate-hexametaphosphate electrolyte with the suspension of SiC nanoparticles [J]. Surface and Coatings Technology, 2015,

276: 266−278.
[36] CHENG Ying-liang, CAO Jin-hui, MAO Mo-ke, XIE Huan-jun, SKELDON P. Key factors determining the development of two morphologies of plasma electrolytic coatings on an Al−Cu−Li alloy in aluminate electrolytes [J]. Surface and Coatings Technology, 2016, 291: 239−249.
[37] LI J F, MAIER B, FRANKEL G S. Corrosion of an Al−Mg−Si alloy under $MgCl_2$ solution droplets [J]. Corrosion Science, 2011, 53: 2142−2151.
[38] YANG J J, BLAWERT C, LAMAKA S V, SNIHIROVA D, LU X P, DI S C, ZHELUDKEVICH M L. Corrosion protection properties of inhibitor containing hybrid PEO-epoxy coating on magnesium [J]. Corrosion Science, 2018, 140: 99−110.
[39] DZHURINSKIY D, GAO Y, YEUNG W K, STRUMBAN E, LESHCHINSKY V, CHU P J, MATTHEWS A, YEROKHIN A, MAEV R G. Characterization and corrosion evaluation of TiO_2: *n*-HA coatings on titanium alloy formed by plasma electrolytic oxidation [J]. Surface and Coatings Technology, 2015, 269: 258−265.
[40] SONG G, ATRENS A, JOHN D S, WU X, NAIRN J. The anodic dissolution of magnesium in chloride and sulphate solutions [J]. Corrosion Science, 1997, 39: 1981−2004.
[41] SONG Guang-ling, SHI Zhi-ming. Corrosion mechanism and evaluation of anodized magnesium alloys [J]. Corrosion Science, 2014, 85: 126−140.
[42] CHEN Jian, WANG Jian-qiu, HAN En-hou, DONG Jun-hua, KE Wei. AC impedance spectroscopy study of the corrosion behavior of an AZ91 magnesium alloy in 0.1M sodium sulfate solution [J]. Electrochimica Acta, 2007, 52: 3299−3309.
[43] SHI X, WANG Y, LI H, ZHANG S, ZHAO R, LI G, ZHANG R, SHENG Y, CAO S, ZHAO Y, XU L, ZHAO Y. Corrosion resistance and biocompatibility of calcium-containing coatings developed in near-neutral solutions containing phytic acid and phosphoric acid on AZ31B alloy [J]. Journal of Alloys and Compounds, 2020, 823: 153721.
[44] CHENG Y L, ZHANG Z, CAO F H, LI J F, ZHANG J Q, WANG J M, CAO C N. A study of the corrosion of aluminum alloy 2024-T3 under thin electrolyte layers [J]. Corrosion Science, 2004, 46: 1649−1667.
[45] HAYNES W M. CRC handbook of chemistry and physics, 95th edition [M]. CRC Press, 2016, 257: 423.
[46] CHENG Ying-liang, CAO Jin-hui, MAO Mo-ke, PENG Zhao-mei, SKELDON P, THOMPSON G E. High growth rate, wear resistant coatings on an Al−Cu−Li alloy by plasma electrolytic oxidation in concentrated aluminate electrolytes [J]. Surface and Coatings Technology, 2015, 269: 74−82.
[47] CHENG Ying-liang, XUE Zhi-gang, WANG Qun, WU Xiang-quan, MATYKINA E, SKELDON P, THOMPSON G E. New findings on properties of plasma electrolytic oxidation coatings from study of an Al−Cu−Li alloy [J]. Electrochimica Acta, 2013, 107: 358−378.
[48] MATYKINA E, ARRABAL R, SCURR D J, BARON A, SKELDON P, THOMPSON G E. Investigation of the mechanism of plasma electrolytic oxidation of aluminium using 18O tracer [J]. Corrosion Science, 2010, 52: 1070−1076.

磁控溅射镀铝 AZ31 镁合金等离子体电解氧化揭示的放电通道结构及其腐蚀行为

胡攀峰，魏兵剑，程昱琳，程英亮

湖南大学 材料科学与工程学院， 长沙 410082

摘　要：在硅酸盐−六偏磷酸盐电解液中对覆盖薄磁控溅射铝层的 AZ31 镁合金进行等离子体电解氧化(PEO)，以研究 PEO 机理并提高合金的耐腐蚀性。使用 SEM 和 EDS 检测涂层形貌并追踪涂层中 Mg 和 Al 元素的分布。新的涂层主要在靠近涂层/金属基体界面的放电通道下部形成。在放电通道上部先前形成的氧化物大部分以固态形式保留在原先的位置，只有少部分熔融氧化物通过涂层的微孔流出，到达表层。阴离子可以通过涂层充满电解液的孔传输，自由地进入涂层的最深部位。在 3.5% NaCl (质量分数)中进行开路电位、极化曲线和 EIS 测试。结果表明，致密的磁控溅射 Al 层可以显着提高 AZ31 镁合金的耐腐蚀性，其耐腐蚀性甚至优于 PEO 处理后的样品。

关键词：AZ31 镁合金；磁控溅射 Al 层；等离子体电解氧化；放电通道；耐腐蚀性能

(Edited by Bing YANG)